Aalto University

OPEN ACCESS

This is an electronic reprint of the original article.
This reprint may differ from the original in pagination and typographic detail.

Du, Luojun; Liao, Mengzhou; Liu, Gui Bin; Wang, Qinqin; Yang, Rong; Shi, Dongxia; Yao, Yugui; Zhang, Guangyu

Strongly distinct electrical response between circular and valley polarization in bilayer transition metal dichalcogenides

Published in:
Physical Review B

DOI:
10.1103/PhysRevB.99.195415

Published: 10/05/2019

Document Version
Publisher's PDF, also known as Version of record

Please cite the original version:
Du, L., Liao, M., Liu, G. B., Wang, Q., Yang, R., Shi, D., Yao, Y., & Zhang, G. (2019). Strongly distinct electrical response between circular and valley polarization in bilayer transition metal dichalcogenides. *Physical Review B*, *99*(19), Article 195415. https://doi.org/10.1103/PhysRevB.99.195415

This material is protected by copyright and other intellectual property rights, and duplication or sale of all or part of any of the repository collections is not permitted, except that material may be duplicated by you for your research use or educational purposes in electronic or print form. You must obtain permission for any other use. Electronic or print copies may not be offered, whether for sale or otherwise to anyone who is not an authorised user.

Strongly distinct electrical response between circular and valley polarization in bilayer transition metal dichalcogenides

Luojun Du,[1,2] Mengzhou Liao,[1] Gui-Bin Liu,[3,*] Qinqin Wang,[1] Rong Yang,[1] Dongxia Shi,[1,4,5] Yugui Yao,[3] and Guangyu Zhang[1,4,5,6,7,†]

[1]*Institute of Physics and Beijing National Laboratory for Condensed Matter Physics, Chinese Academy of Sciences, Beijing 100190, China*
[2]*Department of Electronics and Nanoengineering, Aalto University, Tietotie 3, FI-02150, Finland*
[3]*Beijing Key Laboratory of Nanophotonics and Ultrafine Optoelectronic Systems, School of Physics, Beijing Institute of Technology, Beijing 100081, China*
[4]*School of Physical Sciences, University of Chinese Academy of Science, Beijing 100190, China*
[5]*Beijing Key Laboratory for Nanomaterials and Nanodevices, Beijing 100190, China*
[6]*Collaborative Innovation Center of Quantum Matter, Beijing 100190, China*
[7]*Songshan-Lake Materials Laboratory, Dongguan 523808, Guangdong Province, China*

(Received 17 October 2018; revised manuscript received 24 April 2019; published 10 May 2019)

We introduce a physical model to describe the influence of a perpendicular electric field on circular polarization (CP) and valley polarization (VP) in bilayer transition metal dichalcogenides. Our results uncover that electric-field-dependent CP and VP are quite distinct from each other. The dependence of CP on the electric field harbors a W pattern and possesses the minimum when the potential energy difference between the two layers is equal to the strength of spin-orbit coupling. Such dependence of CP stems from the modulation of energy cost for interlayer hopping and spin-dependent layer polarization. In contrast, VP is strictly absent in primitive bilayers and increases monotonically with increasing strength of electric field, resulting from the continuous variation of valley magnetic moments and inversion-symmetry breaking. Our model elaborates well the recent experimental observations for which the origin is under debate. Moreover, we demonstrate that the manipulation of layer and valley pseudospin is fully tunable by perpendicular electric fields, paving the way for prospects in electrical control of exotic layer-valleytronics.

DOI: 10.1103/PhysRevB.99.195415

I. INTRODUCTION

Monolayer transition metal dichalcogenides (TMDCs) possess a staggered honeycomb lattice structure, and the spatial inversion symmetry is explicitly broken [1,2]. In combination with time-reversal symmetry, monolayer TMDCs harbor valley-contrasting Berry curvature and orbital magnetic moment, leading to valley-selective circular polarization (CP): the interband transition at the $K(K')$ valley couples solely to left (right) circularly polarized light [3–8]. In other words, CP signifies valley polarization (VP) in monolayer TMDCs. Via extrapolating directly the results from monolayer to bilayer without careful discussion, CP was also deemed to denote VP in bilayer $2H$-TMDCs at the initial stage of research [3,5,6,9]. In fact, many practitioners still believe that CP is VP in bilayer TMDCs [10–12]. Since the inversion symmetry is restored in bilayer TMDCs, valley-selective CP is expected to be null. However, robust CP has been observed in a wealth of bilayer TMDCs, e.g., bilayer MoS_2 [5,9,13,14], bilayer WS_2 [12,15], and bilayer WSe_2 [16,17]. This is at odds with our generally believed expectation, indicating that CP may not be VP in bilayer TMDCs. Moreover, strictly zero VP and highly selective CP have been observed simultaneously in bilayer MoS_2 [13], confirming unequivocally that CP cannot signify VP in bilayer TMDCs, in marked contrast to the case of monolayers. For the robust CP in primitive bilayer TMDCs, the origin has been revealed recently via first-principles calculations based on the local effect of spin-orbit physics and is attributed to hidden spin polarization (also referred to as spin-dependent layer polarization) [18,19]. In addition, Gong *et al.* [20] uncovered using $\mathbf{k}\cdot\mathbf{p}$ and tight-binding models that spin-dependent layer polarization is determined by strength of spin-orbit coupling (λ) and interlayer-hopping energy ($t_\perp$). Here, we build on results of Refs. [18,20] and introduce a systematic discussion on the essential difference between CV and VP of bilayer TMDCs, which will play a prominent role in future research and applications.

More importantly, in contrast to the valley physics in monolayer TMDCs that cannot be easily tuned, bilayer TMDCs offer an unprecedented electrically tunable platform for quantum gates and valley-based applications, considering that CP and VP can be continuously tuned by a vertical electric field [9,13,21–23]. A cornucopia of efforts has been paid to underscore the electrical tuning of CP and VP in bilayer TMDCs. Experimental results show that the dependencies on electric field of CP and VP in bilayer TMDCs are quite distinct from each other. VP vanishes when the potential difference between the two layers is null and increases in magnitude with the enhancement of electric field [13]. In marked contrast, robust CP exists at the inversion-symmetry

*Corresponding author: gbliu@bit.edu.cn
†Corresponding author: gyzhang@iphy.ac.cn

 ©2019 American Physical Society

point, decreases in magnitude, goes through a trough, and then increases with increasing strength of perpendicular electric field [9,13]. Such strongly distinct electrical responses of CP and VP are confusing, and the underlying origin has remained elusive. Understanding the physical mechanism is fundamentally important in manipulating CP and VP and in searching for novel electronic applications.

In this paper, we develop a theoretical model to uncover the physics that leads to the different dependencies on electric field of CP and VP. Our results reveal unambiguously that the effect of electric field on CP is quite distinct from that on VP. An electric field perpendicular to the bilayer TMDCs breaks the inversion symmetry and causes the VP to change from 0 under null electric field strength to ± 1 at high field strength. In marked contrast, CP decreases and then increases with increasing strength of electric field, and harbors the minimum when the potential energy difference between the two layers is equal to the strength of spin-orbit coupling (SOC). Our results can explain well the recent experimental observations.

II. WAVE FUNCTIONS OF THE TOP VALENCE BAND

First, we consider the situation without the electric field. In primitive bilayer TMDCs, although interlayer hopping (LH) is suppressed strongly, LH with energy cost between states of upper and lower layers with the same spin can still occur [14,20,24–27], as marked by the magenta bidirectional arrows in Fig. 1(a) and in Fig. S1 of the Supplemental Material [28]. For a given spin, such LH could lead to the states of the top valence band consisting of components of both upper and lower layers, rather than localizing in one layer completely [24,25]. In addition, because of the very large SOC, we could thus construct the wave functions of the top valence band of bilayer TMDCs in terms of monolayer eigenstates [18,20]. For monolayer TMDCs, the wave functions of the valence band maximum are described as follows:

$$\psi_v^m(\tau, s) = \xi_\tau \otimes |s\rangle, \tag{1}$$

where the v (m) indicates valence band (monolayer), $\tau = \pm 1$ denotes the valley index, $s = \pm 1$ is the spin index and indicates spin-up (spin-down) configuration, and ξ_{+1} (ξ_{-1}) represents the orbital state coupled with pure left (right) circularly polarized light [4,18,20]. Accordingly, the twofold-degenerate wave functions of the top valence band in bilayer TMDCs can be written as [Fig. 1(b)]

$$\psi_v^b(\tau, s) = \sum_{l=\pm 1} \beta_{sl}^\tau \xi_{\tau l} |s\rangle, \tag{2}$$

where b denotes bilayer, and $l = \pm 1$ is the layer pseudospin and symbolizes the upper (lower) layer. The squared modulus of coefficient β_{sl}^τ represents the probability and should satisfy the normalization condition:

$$\sum_{l=\pm 1} \left|\beta_{sl}^\tau\right|^2 = 1. \tag{3}$$

In addition, spin-dependent layer polarization can be determined from the probability of wave functions and is

$$\rho_L(\tau, s) = \left|\beta_{sl}^\tau\right|_{l=1}^2 - \left|\beta_{sl}^\tau\right|_{l=-1}^2. \tag{4}$$

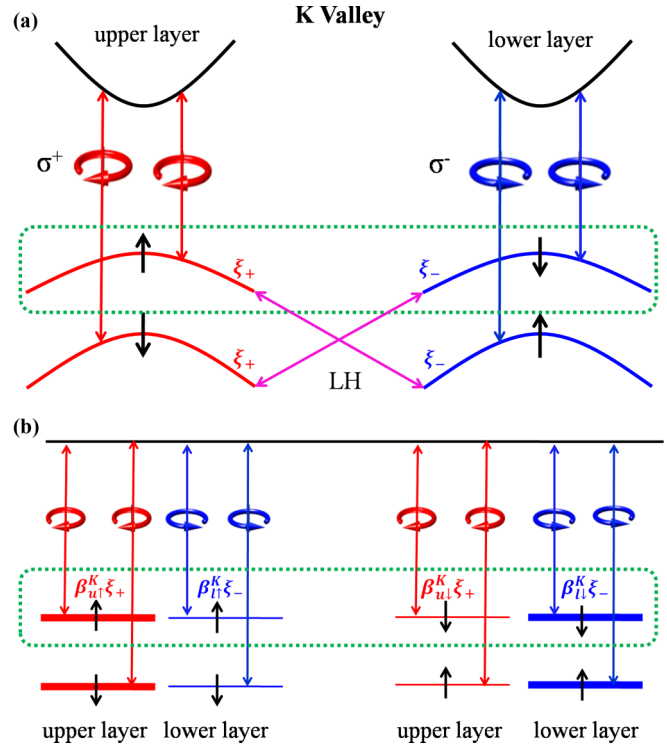

FIG. 1. (a) Schematics of optical transition selection rules in decoupled bilayer TMDCs with $2H$ stacking. Then interlayer hopping is introduced shown as the magenta arrows connecting the same spin states between the upper and lower layers. (b) Optical transition selection rules in the K valley of bilayer TMDCs with interlayer hopping. Red (blue) valance band represents ξ_{+1} (ξ_{-1}) coupled with pure left (right) circularly polarized light. The thickness of the line indicates the probability. Spin configurations are indicated by $\uparrow$ (spin up) and $\downarrow$ (spin down). σ^+ (σ^-) denotes left (right) circularly polarized light (circular arrows).

Recently, Gong *et al.* using the $\mathbf{k}\cdot\mathbf{p}$ model have demonstrated the spin-dependent layer polarization [20]:

$$\rho_L = \tau s \frac{\lambda}{\sqrt{\lambda^2 + t_\perp^2}}. \tag{5}$$

Combining Eqs. (3)–(5), we can obtain the squared modulus of coefficients β_{sl}^τ:

$$\left|\beta_{sl}^\tau\right|^2 = \frac{1}{2} + \tau s l \frac{\lambda}{2\sqrt{\lambda^2 + t_\perp^2}}. \tag{6}$$

III. INTRINSIC CP AND VP

Having identified the wave functions of the top valence band, we then focus on the CP and VP of primitive bilayer TMDCs. To derive the intrinsic CP and VP, we need to take into account the dynamics of photoexcited carriers, i.e., the *absorption*, *relaxation*, and *emission* processes, as illustrated in Fig. 2 and in Fig. S2 of the Supplemental Material [28]. Here we consider the left circularly polarized radiation (σ^+) on resonance with the A exciton. After excitation, the number of photogenerated carriers is proportional to the squared modulus of the transition matrix element $\langle\psi_c|\,\hat{P}_+|\psi_v\rangle$, where

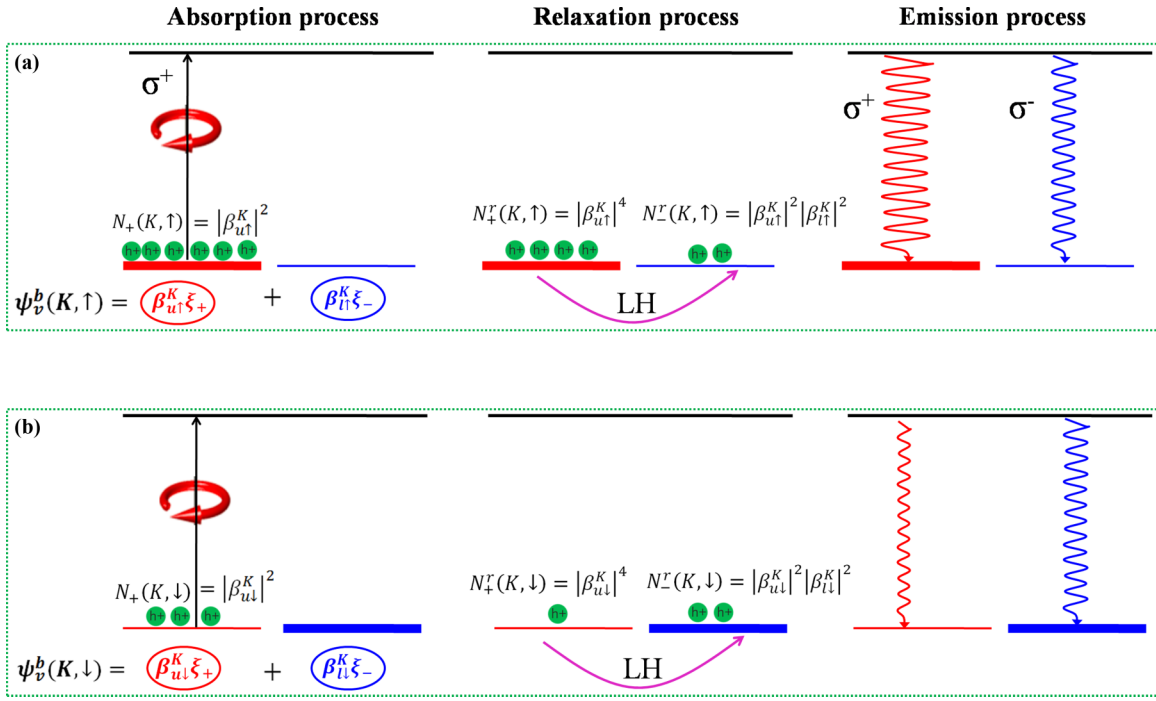

FIG. 2. The dynamics of photoexcited carriers in the K valley for spin-up (a) and spin-down (b) states**.** The twofold-degenerate wave functions of the top valence band of the K valley in TMDC bilayers are described in Eq. (2). Left panel shows absorption process by σ^+ excitation on resonance with the A exciton. The black arrows indicate that the excitation generates holes (green solid ball) with ξ_{+1} character in the valence band. Middle panel denotes the relaxation process via LH. Right panel shows the emission process, filling the holes of the valence band. The red (blue) wavy curves with arrows denote the σ^+ (σ^-) emission, with amplitude representing the relative intensity of emission.

$\hat{P}_\pm = \hat{P}_x \pm i\hat{P}_y$; $\hat{P}_x$ and $\hat{P}_y$ are the x and y components of the momentum operator, respectively [18,29]. Thus, the quantity of photoexcited carriers associated with K and K' valleys can be represented by (Supplemental Material [28])

$$N_+(\tau, s) = \left|\beta^\tau_{sl}\right|^2_{l=\tau}, \tag{7}$$

where the subscript $+$ indicates that photoexcited carriers are associated with σ^+. It can be known from Eq. (7) that only the ξ_{+1} component of the wave functions of the top valence band in K/K' valley is excited. That is to say, photogenerated carriers of the K (K') valley are localized in the upper (lower) layer (left panels of Fig. 2 and of Fig. S2 of the Supplemental Material [28]). Such imbalanced distribution of photoexcited carriers between upper and lower layers will cause the redistribution of holes to restore the eigenstates of the top valence band in the K/K' valley through LH (middle panels of Fig. 2 and Fig. S2), which is the dominant and ultrafast relaxation channel because of the lack of energy barrier (Supplemental Material [28]) [18,30]. Such relaxation process would lead to the photogenerated carriers in the K (K') valley possessing the characters of both ξ_{+1} and ξ_{-1}. After relaxation, the quantities of carriers associated with the K and K' valleys are

$$N^r_+(\tau, s) = \left|\beta^\tau_{sl}\right|^4_{l=\tau}, \quad N^r_-(\tau, s) = \left|\beta^\tau_{sl}\right|^2_{l=\tau} \times \left|\beta^\tau_{sl}\right|^2_{l=-\tau}, \tag{8}$$

where the subscript $+$ ($-$) denotes the carriers associated with σ^+ (σ^-), and r symbolizes the relaxation process.

For the emission process that fills the holes in the valence band (red and blue wavy curve with arrows in the right panels of Fig. 2 and of Fig. S2 of the Supplemental Material [28]), the intensity of photoluminescence (PL) associated with σ^+ (σ^-) is proportional to the number of holes with ξ_{+1} (ξ_{-1}) character. Therefore, we can quantify the CP (ρ_C) and VP (ρ_V) as follows:

$$\rho_C = \frac{N_+ - N_-}{N_+ + N_-}, \quad \rho_V = \frac{N(K) - N(K')}{N(K) + N(K')}, \tag{9}$$

where $N_{+(-)}$ is the total number of carriers associated with σ^+ (σ^-),

$$N_{+(-)} = \sum_{\tau,s} N^r_{+(-)}(\tau, s), \tag{10}$$

and $N(\tau)$ denotes the quantity of carriers in valley τ,

$$N(\tau) = \sum_s [N^r_+(\tau, s) + N^r_-(\tau, s)]. \tag{11}$$

According to Eqs. (6)–(11), we can obtain the intrinsic VP and CP of primitive bilayer TMDCs:

$$\rho_C = \frac{\lambda^2}{\lambda^2 + t_\perp^2} = (\rho_L)^2, \tag{12}$$

$$\rho_V = 0. \tag{13}$$

Our results reveal clearly the difference between the VP and CP in primitive bilayer TMDCs. VP in TMDC bilayers is strictly absent, in good harmony with the global inversion symmetry [3,13,31]. In marked contrast, TMDC bilayers can harbor intrinsic nonzero CP. The intrinsic CP turns out to

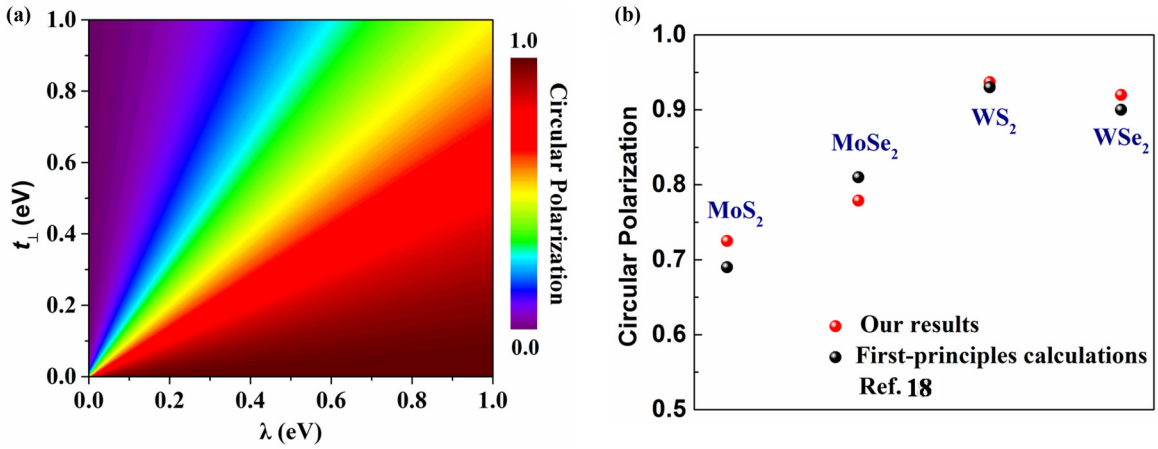

FIG. 3. (a) CP as a function of spin-orbit coupling λ and interlayer hopping $t_\perp$. (b) CP of TMDC bilayers calculated by our model (red symbols), compared to first-principles calculations (black symbols).

be equal to the square of spin-dependent layer polarization, in good agreement with the results presented in Ref. [18]. Furthermore, our results demonstrate that the intrinsic CP in bilayer TMDCs is determined by two intrinsic physical characteristic parameters (λ and $t_\perp$) and show a clear physical picture of intrinsic CP. In addition, using the values of λ and $t_\perp$ that have been determined via experiment and theory, we can obtain the intrinsic CP of bilayer TMDCs quickly and easily, without the help of a computer server, which is deemed essential for first-principles calculations. Figure 3(a) shows the CP as a function of λ and $t_\perp$. The stronger λ and smaller $t_\perp$ would lead to larger CP. The very large SOC in bilayer TMDCs, especially for bilayer WS_2, has allowed us to observe robust CP [11,12,15]. Figure 3(b) presents the CP of bilayer TMDCs calculated by Eq. (12) with the values of λ and $t_\perp$ in Ref. [20], in fair agreement with the first-principles calculations [18]. On the other hand, it can be seen that the results of our model and first-principles calculations in Ref. [18] are not completely identical. Such small difference stems from that the band structure, λ, and $t_\perp$ derived from distinct theoretical calculations show some differences [24,29], rather than the accuracy of our model. In fact, for the intrinsic CP of bilayer TMDCs, our results and the first-principles calculations in Ref. [18] are completely equivalent and possess the same accuracy, with the details listed in the Supplemental Material [28]. Compared with Ref. [18], the distinction of our work is as follows. First, we introduce two intrinsic physical characteristic parameters into our physical model, i.e., λ and $t_\perp$. Thus, we can obtain the clear physical picture and gain the CP and VP easily, without the help of a computer server. Second, our results reveal clearly both the zero VP and the essential difference between the VP and CP in primitive bilayer TMDCs, so that researchers will not confuse them. Third, our work uncovers the physical mechanism of the strongly distinct electrical response between CP and VP. This is the main goal of our work, as discussed in detail below.

IV. ELECTRIC-FIELD-DEPENDENT CP AND VP

After elucidating the difference between CP and VP in bilayer TMDCs, we then explain the physical mechanism that gives rise to the strongly distinct electrical response between CP and VP. Since the maximum potential difference between upper and lower layers is about 100 meV under experimental conditions [13], we consider the situation of a small electric field, and the influence of the electric field on the exciton energy and spin splitting can be ignored. Thus, we can determine the electric-field-dependent CP and VP, being akin to the case without the electric field. When we apply an electric field (E) perpendicular to the bilayer TMDCs [Fig. 4(a)], the out-of-plane electric field introduces an energy difference, i.e., eEd, between the upper and lower layer, where e and d denote the elementary charge and interlayer distance, respectively [Fig. 4(b)]. Therefore, both the energy cost for LH and spin-dependent layer polarization will change. The energy cost of LH is λ for both spin-up and spin-down states when the electric field is absent [Fig. 1(a)]. In contrast, the energy cost for LH under a vertical electric field changes to $\lambda + \tau seEd$ (Fig. 4(b) and Fig. S3 of the Supplemental Material [28]). Correspondingly, the spin-dependent layer polarization changes to

$$\rho_L(\tau, s) = \left|\beta_{sl}^{\tau}\right|_{l=1}^2 - \left|\beta_{sl}^{\tau}\right|_{l=-1}^2 = \tau s \frac{\lambda + \tau seEd}{\sqrt{(\lambda + \tau seEd)^2 + t_\perp^2}}. \tag{14}$$

In conjunction with the normalization condition Eq. (3), we can derive the squared modulus of coefficients under a vertical electric field:

$$\left|\beta_{sl}^{\tau}\right|^2 = \frac{1}{2} + \tau sl \frac{\lambda + \tau seEd}{2\sqrt{(\lambda + \tau seEd)^2 + t_\perp^2}}. \tag{15}$$

In combination with Eqs. (8)–(11), we thus can obtain the electric-field-dependent CP and VP as follows:

$$\rho_C = \frac{N_+ - N_-}{N_+ + N_-} = \frac{1}{2}\left[\frac{(\lambda + eEd)^2}{(\lambda + eEd)^2 + t_\perp^2} + \frac{(\lambda - eEd)^2}{(\lambda - eEd)^2 + t_\perp^2}\right], \tag{16}$$

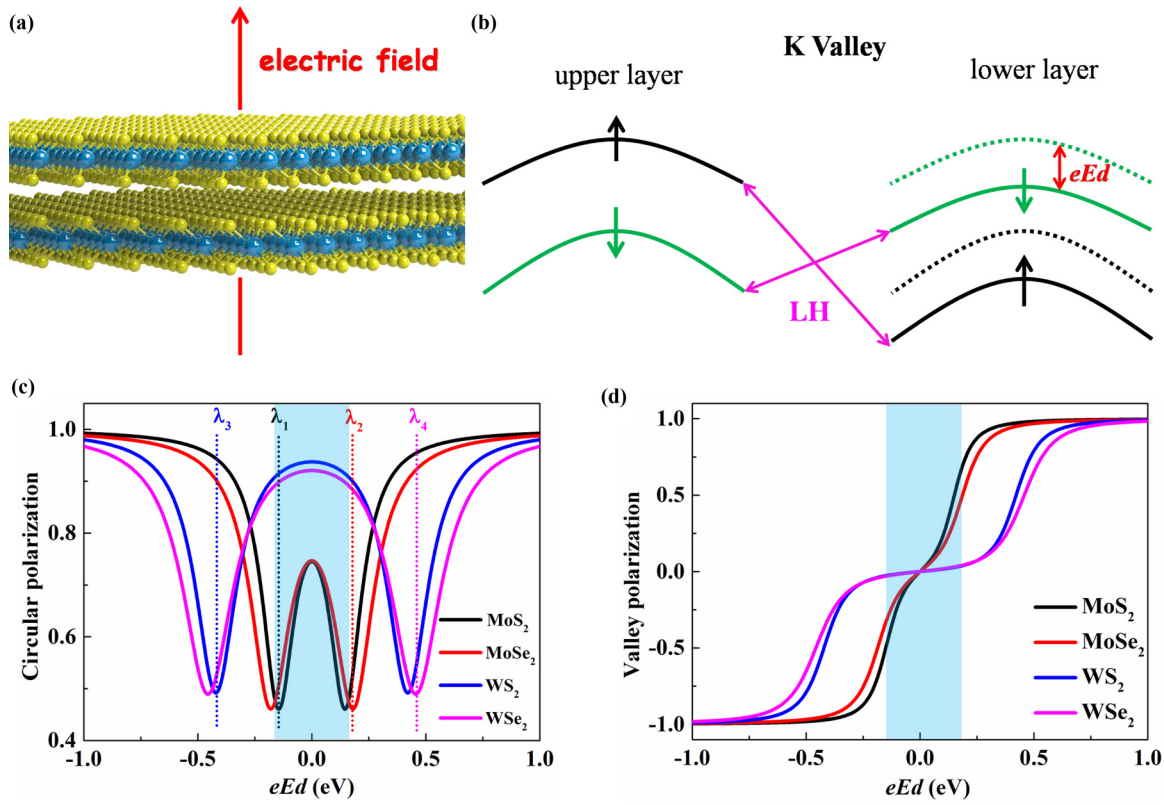

FIG. 4. (a) Schematic illustration of the 2*H*-TMDC bilayer with an out-of-plane electric field E. (b) Schematic diagram of the valence band structure under a perpendicular electric field. The electric field introduces an energy difference between the upper and lower layer: eEd. Dotted valence band structure is the situation without electric field. (c) Circular polarization as a function of electric field. λ_1, λ_2, λ_3, and λ_4 are the strength of SOC for MoS_2, $MoSe_2$, WS_2, and WSe_2, respectively. (d) Valley polarization versus the electric field. The region highlighted by light blue denotes the potential energy differences allowed by the experimental conditions.

$$\rho_V = \frac{N(K) - N(K')}{N(K) + N(K')} = \frac{1}{2}\left[\frac{\lambda + eEd}{\sqrt{(\lambda + eEd)^2 + t_\perp^2}} - \frac{\lambda - eEd}{\sqrt{(\lambda - eEd)^2 + t_\perp^2}}\right]. \quad (17)$$

Figures 4(c) and 4(d) show the CP and VP as a function of potential energy differences (eEd) between the upper and lower layers. It can be seen clearly that the electrical responses of CP and VP are strongly distinct from each other. Taking MoS_2 as an example, the evolutions of CP and VP with electric field have been determined by experiments (Supplemental Material [28]) [9,13]. Within the potential energy differences allowed by the experimental conditions [highlighted by light blue in Figs. 4(c) and 4(d)], CP harbors a W pattern and possesses the minimum when eEd is equal to SOC. In stark contrast, VP increases monotonically with increasing strength of electric field. Our results elaborate successfully the recent experimental observations for which the origin is unclear and confusing. It should be noted that the drop of VP under large negative gate voltage and asymmetry of CP about the inversion-symmetry point in Ref. [13] originates from the decline in electron density and screening of the electric field, respectively, since MoS_2 is an n-type semiconductor [32–35]. Furthermore, we see from Figs. 4(c) and 4(d) that both the CP and VP of WS_2 and WSe_2, as compared with MoS_2 and $MoSe_2$, cannot be easily tuned under experimental conditions due to the strong SOC. This is in fair agreement with the recent results that the CP of WS_2 is almost independent of perpendicular electric field [15].

Compared with experimental results, our results possess a relatively high value of CP and VP for bilayer TMDCs. This is due to that for the actual experiments, the TMDCs cannot be perfect and would possess a high density of vacancies (for instance, defect density can reach 3.5×10^{13} cm^{-2}) [36] and some extrinsic irregularities induced by dangling bonds, charge traps, and impurities of substrate [37,38]. Thus, intervalley relaxation induced by an exchange mechanism (Maialle-Silva-Sham mechanism) would play a key role for CP, leading the CP to be less than unity [30,39–43]. Taking the intervalley relaxation into account, the CP and VP of monolayer TMDCs can be denoted as ρ_{EM}. For bilayer TMDCs, in addition to the intervalley relaxation, they also possess the relaxation channel of LH. For the intervalley relaxation of bilayer TMDCs, this has the same mechanism as the monolayer. If we only consider the intervalley relaxation, the CP or VP of bilayer TMDCs is ρ_{EM}. If we only consider the relaxation channel of LH, the CP (VP) of bilayer TMDCs is $\rho_{\mathrm{LH}}^{\mathrm{CP}}$ ($\rho_{\mathrm{LH}}^{\mathrm{VP}}$). Since the relaxation channel of LH and intervalley relaxation are independent of each other, the CP (VP) of bilayer TMDCs

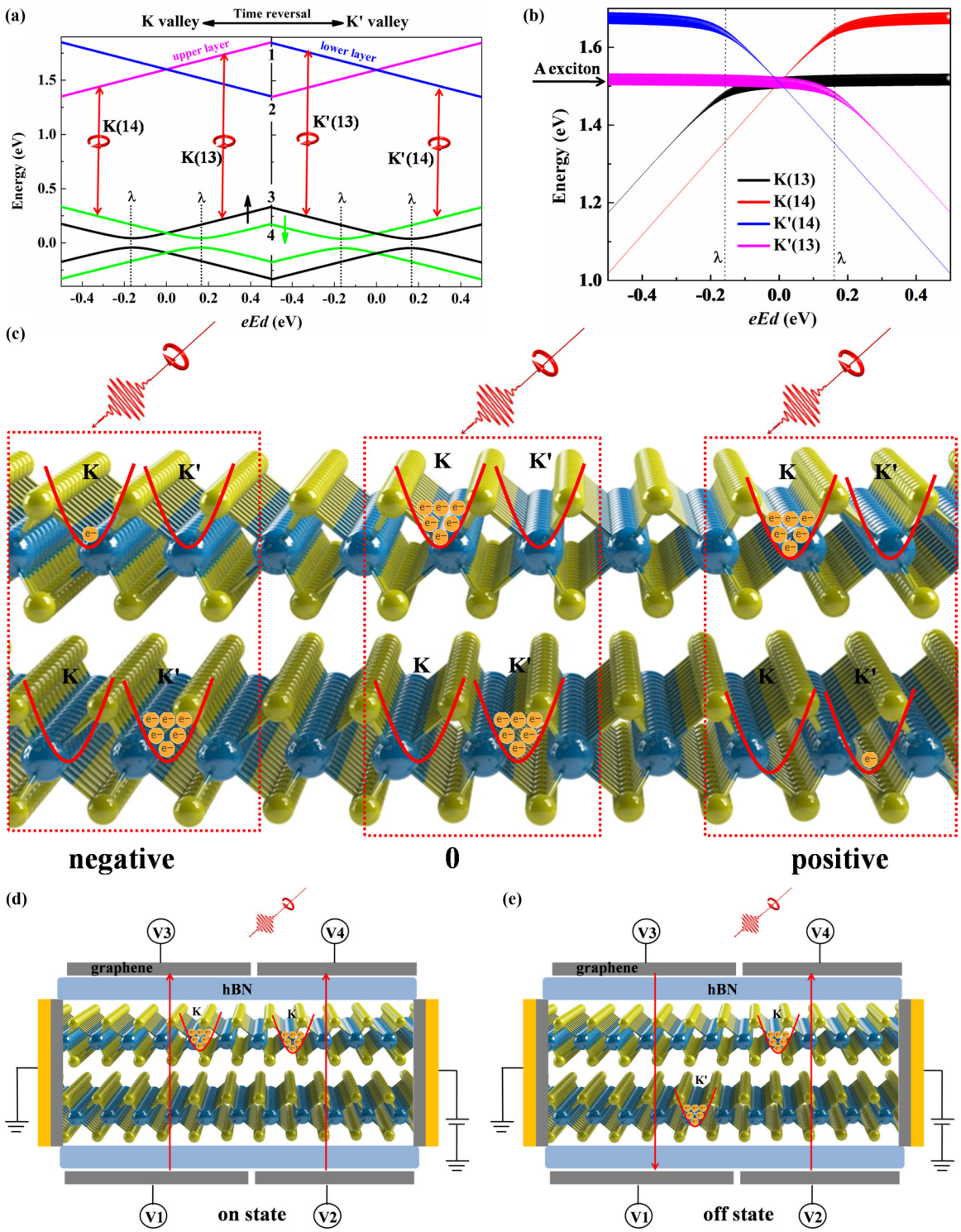

FIG. 5. (a) Electric-field-dependent band structure of K and K' valleys from $\mathbf{k}\cdot\mathbf{p}$ model for bilayer MoS_2. Δ, λ, and $t_\perp$ are 1.6 eV, 147 meV, and 86 meV. (b) Optical transition energy as a function of electric field. Linewidth is proportional to the population of σ^+ in corresponding wave function. (c) Schematic diagram of the layer-valley-dependent excitation processes under negative (left), zero (middle), and positive (right) electric field. Positive electric field denotes the direction of electric field from the lower layer to upper layer. (d), (e) Schematic diagram of electrical control of layer-valleytronics for on state (d) and off state (e).

will be $\rho_{EM} \times \rho_{\mathrm{LH}}^{\mathrm{CP}}$ ($\rho_{\mathrm{LH}}^{\mathrm{VP}}$) under both the relaxation channel of LH and intervalley relaxation. Due to the relaxation channel of LH, CP (VP) of bilayer TMDCs is smaller than that of the monolayer, in good agreement with experimental results [14]. Moreover, intervalley relaxation is independent of the electric field; the strongly distinct electrical responses of CP and VP are thus determined by only the relaxation channel of LH. Intervalley relaxation does not affect the clarification

of physical mechanisms and only produces a correction factor ρ_{EM} on our results. Thus, we ignore the intervalley relaxation in our paper.

V. ELECTRICAL CONTROL OF LAYER-VALLEYTRONICS

In order to understand the electric-field-driven evolution of CP and VP more clearly, we performed calculations through the $\mathbf{k}\cdot\mathbf{p}$ model with MoS_2 as an example. Figure 5(a) shows the energies of the K and K' valleys versus the electric fields through the $\mathbf{k}\cdot\mathbf{p}$ model for bilayer MoS_2 (Supplemental Material [28]). One can see explicitly the emergence of a kink in the valence band when eEd is equal to λ, indicating the relatively strongest LH and smallest layer polarization [44]. Since CP stems from layer polarization, it would possess the trough. As eEd gradually moves away from λ (whether increasing or decreasing), the energy cost for LH becomes larger, giving rise to a stronger CP and W-shaped pattern.

Due to the large valence band spin splitting, we focus only on the two higher-lying states at the valence band edge. Under σ^+ excitation, electron-hole pairs via four transitions, as illustrated by red double arrows in Fig. 5(a), can be excited [16,20]. Two of the transitions associated with the K (K') valley come from the upper (lower) layer. Figure 5(b) presents the electric-field-driven evolution of energies for these four optical transitions. The linewidth denotes the strength of the corresponding transition, which is the squared modulus of coefficients calculated via Eq. (15) with λ and $t_\perp$ of MoS_2. Here, we consider the σ^+ radiation with energy that is equal to the energy of the A exciton of the monolayer, as illustrated in Fig. 5(b). In fact, resonant excitation with the A exciton is the condition used in most experimental measurements [5,6,9,13]. When eEd is zero, the transition $K(13)$ [$K(14)$] associated with the K valley plays the same role as the transition $K'(13)$ [$K'(14)$] associated with the K' valley. This means that the photoexcited carriers are the same between K and K' valleys, leading to the zero VP. With increasing eEd, the intrinsic inversion symmetry is broken; transitions $K(13)$ [$K'(13)$] stemming from the upper (lower) layer will play a dominant role for positive (negative) electric fields. Thus, photoexcited carriers will be concentrated mainly in K (K') valleys under positive (negative) electric fields, giving rise to the observable VP. The larger the electric field is, the greater the VP would be. Thus, we observe the continuous variation of VP. To further clarify the physical origin of the VP, we calculate the electric-field-dependent orbital magnetic moments and Berry curvatures via the $\mathbf{k}\cdot\mathbf{p}$ model, which are two physical quantities and characterize the valley physics [1,3,34,45,46]. The orbital magnetic moments ($\boldsymbol{m}$) of the K valley are as follows (Supplemental Material [28]) [1,20]:

$$\boldsymbol{m} = \frac{ea^2t^2}{\hbar\Delta}\left[\frac{\lambda - eEd}{\sqrt{(\lambda - eEd)^2 + t_\perp^2}} - \frac{\lambda + eEd}{\sqrt{(\lambda + eEd)^2 + t_\perp^2}}\right], \tag{18}$$

where Δ, $\hbar$, a, and t are the energy gap, reduced Planck constant, lattice constant, and nearest-neighbor intralayer hopping, respectively. In conjunction with Eq. (17), it can be known unequivocally that the VP is proportional to $\boldsymbol{m}$, in fair agreement with previous results [3,9,13]:

$$\rho_V = -\frac{\boldsymbol{m}}{\mu_B^*}, \quad \mu_B^* = \frac{e\hbar}{2m^*} = -\frac{2ea^2t^2}{\hbar\Delta}, \tag{19}$$

where μ_B^* is the effective Bohr magneton with the bare electron mass replaced by the effective mass m^*.

More importantly, the vertical electric field offers an approach to manipulating the layer and valley pseudospin. From Fig. 5(b), we see that both the K valley of upper layer [transition $K(13)$] and K' valley of lower layer [transition $K'(13)$] are excited simultaneously under null electric field, as illustrated by the middle panels in Fig. 5(c). In stark contrast, the K valley of the upper layer (K' valley of the lower layer) is mainly excited under positive (negative) electric fields, as illustrated by the right (left) of Fig. 5(c). Such layer-valley locking allows us to develop exotic optoelectronics. As shown in Figs. 5(d) and 5(e), the vertical electric field on both the left and right can be tuned by voltages V1–V4. When the directions of the electric field are the same between the left and right (for example, both are positive), the K valley of the upper layer will be excited on both the left and right [Fig. 5(d)]. If we apply a voltage between the source (metal pad on left) and drain (metal pad on right), photoexcited carriers can flow easily from left to right and we can obtain a low-resistance state (the "on state"). When the directions of the electric field are opposite between the left and right (for instance, left is negative while right is positive), the K (K') valley of the upper (lower) layer will be excited on the right (left) [Fig. 5(e)]. Since both intervalley scattering between the K and K' valleys and LH between the upper and lower layers are strongly suppressed due to very large SOC, it is almost impossible for photoexcited carriers to flow from left to right and we could obtain a high-resistance state (the "off state"). Such two distinct resistance states can be regarded as "1" (on state) and "0" (off state) and could be used for quantum logic devices. Electrical tuning of layer and valley pseudospin in bilayer TMDCs provides an unprecedented platform to shed light on engineering of layer-valleytronics.

VI. CONCLUSIONS

To summarize, we have explained the difference between CP and VP in bilayer TMDCs. The CP stems from the spin-dependent layer polarization and shows a W pattern with perpendicular electric field. In contrast, the VP is governed by the global inversion symmetry and can be continuously tuned by the potential difference between the two layers. Such quite distinct responses to the electric field can elaborate well the recent experimental results that are unclear and confusing. Moreover, our work elaborates the importance of the electrical field in the manipulation of CP and VP and paves a way towards the electrical control of quantum logic and layer-valleytronics applications based on bilayer TMDCs.

ACKNOWLEDGMENTS

We acknowledge Uddin Md Gius for fully checking the manuscript. G.Z. thanks the National Science Foundation of China (NSFC) under Grant No. 11834017, the National Key R&D Program under Grant No. 2016YFA0300904, the

Strategic Priority Research Program of the Chinese Academy of Sciences (CAS) under Grant No. XDB30000000, and the Key Research Program of Frontier Sciences of the CAS under Grant No. QYZDB-SSW-SLH004. D.S. thanks the National Science Foundation of China (NSFC) under Grants No. 61734001 and No. 51572289. R.Y. thanks the Youth Innovation Promotion Association of the CAS under Grant No. 2018013. G.-B.L. thanks the National Key R&D Program of China under Grant No. 2017YFB0701600 and the NSFC under Grant No. 11304014.

[1] D. Xiao, G.-B. Liu, W. Feng, X. Xu, and W. Yao, Phys. Rev. Lett. **108**, 196802 (2012).
[2] G.-B. Liu, W.-Y. Shan, Y. Yao, W. Yao, and D. Xiao, Phys. Rev. B **88**, 085433 (2013).
[3] W. Yao, D. Xiao, and Q. Niu, Phys. Rev. B **77**, 235406 (2008).
[4] T. Cao, G. Wang, W. Han, H. Ye, C. Zhu, J. Shi, Q. Niu, P. Tan, E. Wang, B. Liu, and J. Feng, Nat. Commun. **3**, 887 (2012).
[5] K. F. Mak, K. He, J. Shan, and T. F. Heinz, Nat. Nanotechnol. **7**, 494 (2012).
[6] H. Zeng, J. Dai, W. Yao, D. Xiao, and X. Cui, Nat. Nanotechnol. **7**, 490 (2012).
[7] G. Sallen, L. Bouet, X. Marie, G. Wang, C. R. Zhu, W. P. Han, Y. Lu, P. H. Tan, T. Amand, B. L. Liu, and B. Urbaszek, Phys. Rev. B **86**, 081301(R) (2012).
[8] X. Xu, W. Yao, D. Xiao, and T. F. Heinz, Nat. Phys. **10**, 343 (2014).
[9] S. Wu, J. S. Ross, G.-B. Liu, G. Aivazian, A. Jones, Z. Fei, W. Zhu, D. Xiao, W. Yao, D. Cobden, and X. Xu, Nat. Phys. **9**, 149 (2013).
[10] Y. Wang, C. Cong, J. Shang, M. Eginligil, G. Li, Y. Chen, N. Peimyoo, and T. Yu, Nanoscale Horiz. **4**, 396 (2019).
[11] H. Su, C. Wei, A. Deng, D. Deng, C. Yang, and J.-F. Dai, Nanoscale **9**, 5148 (2017).
[12] P. K. Nayak, F.-C. Lin, C.-H. Yeh, J.-S. Huang, and P.-W. Chiu, Nanoscale **8**, 6035 (2016).
[13] J. Lee, K. F. Mak, and J. Shan, Nat. Nanotechnol. **11**, 421 (2016).
[14] R. Suzuki, M. Sakano, Y. J. Zhang, R. Akashi, D. Morikawa, A. Harasawa, K. Yaji, K. Kuroda, K. Miyamoto, T. Okuda, K. Ishizaka, R. Arita, and Y. Iwasa, Nat. Nanotechnol. **9**, 611 (2014).
[15] B. Zhu, H. Zeng, J. Dai, Z. Gong, and X. Cui, Proc. Natl. Acad. Sci. USA **111**, 11606 (2014).
[16] A. M. Jones, H. Yu, J. S. Ross, P. Klement, N. J. Ghimire, J. Yan, D. G. Mandrus, W. Yao, and X. Xu, Nat. Phys. **10**, 130 (2014).
[17] G. Wang, X. Marie, L. Bouet, M. Vidal, A. Balocchi, T. Amand, D. Lagarde, and B. Urbaszek, Appl. Phys. Lett. **105**, 182105 (2014).
[18] Q. Liu, X. Zhang, and A. Zunger, Phys. Rev. Lett. **114**, 087402 (2015).
[19] X. Zhang, Q. Liu, J.-W. Luo, A. J. Freeman, and A. Zunger, Nat. Phys. **10**, 387 (2014).
[20] Z. Gong, G.-B. Liu, H. Yu, D. Xiao, X. Cui, X. Xu, and W. Yao, Nat. Commun. **4**, 2053 (2013).
[21] J. Klein, J. Wierzbowski, A. Steinhoff, M. Florian, M. Rösner, F. Heimbach, K. Müller, F. Jahnke, T. O. Wehling, J. J. Finley, and M. Kaniber, Nano Lett. **17**, 392 (2016).
[22] A. Kormányos, V. Zólyomi, V. I. Fal'ko, and G. Burkard, Phys. Rev. B **98**, 035408 (2018).
[23] Q. Tong, H. Yu, Q. Zhu, Y. Wang, X. Xu, and W. Yao, Nat. Phys. **13**, 356 (2017).
[24] L. Du, T. Zhang, M. Liao, G. Liu, S. Wang, R. He, Z. Ye, H. Yu, R. Yang, D. Shi, Y. Yao, and G. Zhang, Phys. Rev. B **97**, 165410 (2018).
[25] X. Fan, D. J. Singh, and W. Zheng, J. Phys. Chem. Lett. **7**, 2175 (2016).
[26] A. Arora, M. Koperski, A. Slobodeniuk, K. Nogajewski, R. Schmidt, R. Schneider, M. R Molas, S. M. de Vasconcellos, and R. Bratschitsch, 2D Mater. **6**, 015010 (2018).
[27] Y. Wang, Z. Wang, W. Yao, G.-B. Liu, and H. Yu, Phys. Rev. B **95**, 115429 (2017).
[28] See Supplemental Material at http://link.aps.org/supplemental/10.1103/PhysRevB.99.195415 for further information concerning wave functions of the top valence band in the K′ valley of primitive bilayers, transition matrix elements, the absorption process, justification for the ultrafast relaxation model, the squared modulus of the coefficient associated with the K′ valley under a perpendicular electric field, orbital magnetic moments and Berry curvatures under a vertical electric field, and the equivalence between our models and first-principles calculations.
[29] G.-B. Liu, D. Xiao, Y. Yao, X. Xu, and W. Yao, Chem. Soc. Rev. **44**, 2643 (2015).
[30] J. Kim, C. Jin, B. Chen, H. Cai, T. Zhao, P. Lee, S. Kahn, K. Watanabe, T. Taniguchi, S. Tongay, M. F. Crommie, and F. Wang, Sci. Adv. **3**, e1700518 (2017).
[31] D. Xiao, W. Yao, and Q. Niu, Phys. Rev. Lett. **99**, 236809 (2007).
[32] B. Radisavljevic, A. Radenovic, J. Brivio, V. Giacometti, and A. Kis, Nat. Nanotechnol. **6**, 147 (2011).
[33] L. Xie, M. Liao, S. Wang, H. Yu, L. Du, J. Tang, J. Zhao, J. Zhang, P. Chen, X. Lu, G. Wang, G. Xie, R. Yang, D. Shi, and G. Zhang, Adv. Mater. **29**, 1702522 (2017).
[34] K. F. Mak, K. L. McGill, J. Park, and P. L. McEuen, Science **344**, 1489 (2014).
[35] X. Cui, G.-H. Lee, Y. D. Kim, G. Arefe, P. Y. Huang, C.-H. Lee, D. A. Chenet, X. Zhang, L. Wang, F. Ye, F. Pizzocchero, B. S. Jessen, K. Watanabe, T. Taniguchi, D. A. Muller, T. Low, P. Kim, and J. Hone, Nat. Nanotechnol. **10**, 534 (2015).
[36] J. Hong, Z. Hu, M. Probert, K. Li, D. Lv, X. Yang, L. Gu, N. Mao, Q. Feng, L. Xie, J. Zhang, D. Wu, Z. Zhang, C. Jin, W. Ji, X. Zhang, J. Yuan, and Z. Zhang, Nat. Commun. **6**, 6293 (2015).
[37] F. Cadiz, E. Courtade, C. Robert, G. Wang, Y. Shen, H. Cai, T. Taniguchi, K. Watanabe, H. Carrere, D. Lagarde, M. Manca, T. Amand, P. Renucci, S. Tongay, X. Marie, and B. Urbaszek, Phys. Rev. X **7**, 021026 (2017).
[38] Y. Y. Illarionov, G. Rzepa, M. Waltl, T. Knobloch, A. Grill, M. M. Furchi, T. Mueller, and T. Grasser, 2D Mater. **3**, 035004 (2016).
[39] K. Hao, G. Moody, F. Wu, C. K. Dass, L. Xu, C.-H. Chen, L. Sun, M.-Y. Li, L.-J. Li, A. H. MacDonald, and X. Li, Nat. Phys. **12**, 677 (2016).

[40] T. Yu and M. W. Wu, Phys. Rev. B **89**, 205303 (2014).
[41] T. Yu and M. W. Wu, Phys. Rev. B **93**, 045414 (2016).
[42] L. Du, Q. Zhang, B. Gong, M. Liao, J. Zhu, H. Yu, R. He, K. Liu, R. Yang, D. Shi, L. Gu, F. Yan, G. Zhang, and Q. Zhang, Phys. Rev. B **97**, 115445 (2018).
[43] T. Jakubczyk, V. Delmonte, M. Koperski, K. Nogajewski, C. Faugeras, W. Langbein, M. Potemski, and J. Kasprzak, Nano Lett. **16**, 5333 (2016).
[44] S. Gao, L. Yang, and C. D. Spataru, Nano Lett. **17**, 7809 (2017).
[45] M. Sui, G. Chen, L. Ma, W.-Y. Shan, D. Tian, K. Watanabe, T. Taniguchi, X. Jin, W. Yao, D. Xiao, and Y. Zhang, Nat. Phys. **11**, 1027 (2015).
[46] R. Gorbachev, J. C. W. Song, G. L. Yu, A. V. Kretinin, F. Withers, Y. Cao, A. Mishchenko, I. V. Grigorieva, K. S. Novoselov, L. S. Levitov, and A. K. Geim, Science **346**, 448 (2014).